Research Article

Journal of Molecular Recognition

Received: 16 March 2012, Revised: 16 November 2012, Accepted: 12 December 2012, Published online in Wiley Online Library

(wileyonlinelibrary.com) DOI: 10.1002/jmr.2261

Importance of the interaction protein–protein of the CaM–PDE1A and CaM–MLCK complexes in the development of new anti-CaM drugs

Martin González-Andrade[a,b]*, Rachel Mata[b], Abraham Madariaga-Mazón[b], Rogelio Rodríguez-Sotres[b], Luis del Pozo-Yauner[a] and Alejandro Sosa-Peinado[c]

Protein–protein interactions play central roles in physiological and pathological processes. The bases of the mechanisms of drug action are relevant to the discovery of new therapeutic targets. This work focuses on understanding the interactions in protein–protein–ligands complexes, using proteins calmodulin (CaM), human calcium/calmodulin-dependent 3′,5′-cyclic nucleotide phosphodiesterase 1A active human (PDE1A), and myosin light chain kinase (MLCK) and ligands αII–spectrin peptide (αII–spec), and two inhibitors of CaM (chlorpromazine (CPZ) and malbrancheamide (MBC)). The interaction was monitored with a fluorescent biosensor of CaM (*h*CaM M124C–*mBBr*). The results showed changes in the affinity of CPZ and MBC depending on the CaM–protein complex under analysis. For the Ca^{2+}–CaM, Ca^{2+}–CaM–PDE1A, and Ca^{2+}–CaM–MLCK complexes, CPZ apparent dissociation constants (K_{ds}) were 1.11, 0.28, and 0.55 μM, respectively; and for MBC K_{ds} were 1.43, 1.10, and 0.61 μM, respectively. In competition experiments the addition of calmodulin binding peptide 1 (αII–spec) to Ca^{2+}–*h*CaM M124C–*mBBr* quenched the fluorescence ($K_d = 2.55 \pm 1.75$ pM) and the later addition of MBC (up to 16 μM) did not affect the fluorescent signal. Instead, the additions of αII–spec to a preformed Ca^{2+}–*h*CaM M124C–*mBBr*–MBC complex modified the fluorescent signal. However, MBC was able to displace the PDE1A and MLCK from its complex with Ca^{2+}–CaM. In addition, docking studies were performed for all complexes with both ligands showing an excellent correlation with experimental data. These experiments may help to explain why *in vivo* many CaM drugs target prefer only a subset of the Ca^{2+}–CaM regulated proteins and adds to the understanding of molecular interactions between protein complexes and small ligands. Copyright © 2013 John Wiley & Sons, Ltd.

Supporting information may be found in the online version of this paper.

Keywords: αII–spec; calmodulin; malbrancheamide; protein–protein interactions; protein–peptide interactions

INTRODUCTION

Protein–protein interactions regulate a wide variety of important cellular pathways and represent frequent targets for drug discovery. Modern proteomic studies continue revealing new protein–protein interactions involved in the control of various physiological and pathological processes (Rimmele *et al*., 2010). Hence, the identification of molecules interacting specifically with multisite proteins or with protein–protein complexes is of great interest (Oboyle and Waddington, 1985; Buchwald *et al*., 2010). One of these proteins is calmodulin (CaM), the major transducer of Ca^{2+} signals. This protein has no enzymatic activity but acts in response to Ca^{2+} concentration to modulate a wide variety of target proteins and through these interactions regulates a large number of biochemical processes (Sorensen and Shea, 1998). Therefore, CaM is an excellent system for studying the mechanism of drugs action, targeting to protein–protein complexes. CaM is an intracellular highly conserved protein ubiquitous in eukaryotic cells, which possesses two Ca^{2+}-binding domains connected by a flexible linker. Upon Ca^{2+} binding, this protein exposes its hydrophobic patches and makes possible its binding to more than 300 target proteins (Junker and Rief, 2009), with affinities in the nanomolar to micromolar range. Examples of CaM-sensitive proteins are *c*AMP phosphodiesterase 1 (PDE1; Goraya and Cooper, 2005), adenylyl cyclases 1 and 8 (Wang and Storm, 2003), myosin light chain kinase (MLCK) (Webb, 2003), Ca^{2+}/calmodulin protein kinase II (Evans and Shea, 2009), CaM kinase I–IV (Nairn and Picciotto, 1994), calcineurin (Aramburu *et al*., 2000), nitric oxide synthase (Cho *et al*., 1992; Xia and Storm, 2005), caldesmon (Huber *et al*., 1996), and spectrin (Bjork *et al*., 1995). Ca^{2+}–CaM target complexes play key roles in many cellular processes such as transcription, protein synthesis, fast axonal transport, smooth muscle contraction, secretion, organelle tubulation, ion channel function, cellular proliferation, and the chemotaxis to mention some of them (Hait and Lazo, 1986; Chin and Means, 2000; Du *et al*., 2004; Bouche *et al*., 2005; Seales *et al*., 2006).

* *Correspondence to: Martin González-Andrade, Instituto Nacional de Medicina Genómica, Secretaría de Salud, México DF 14610, México.*
E-mail: mgonzalez@inmegen.gob.mx

a *M. González-Andrade, L. Pozo-Yauner*
Instituto Nacional de Medicina Genómica, Secretaría de Salud, México DF 14610, México

b *M. González-Andrade, R. Mata, A. Madariaga-Mazón, R. Rodríguez-Sotres*
Facultad de Química, Universidad Nacional Autónoma de México, México DF 04510, México

c *A. Sosa-Peinado*
Facultad de Medicina, Universidad Nacional Autónoma de México, México DF 04510, México

The enzyme PDE1 plays a crucial role in degradation of adenosine 3′-5′-monophosphate (*c*AMP), an important second messenger (Beavo, 1995). After the discovery of PDE1 role in signal transduction, this protein was identified as a therapeutic target, on the grounds of a basic pharmacological principle; that is, a modulation of the degradation of a second messenger can make often a quicker and longer-lasting effect than a comparable modulation of the rates of its synthesis. Accordingly, the inhibition of CaM-mediated activation of PDE1 has been related with the therapeutic smooth muscle relaxant effect of some drugs (Masciarelli *et al*., 2004).

Another protein of big interest and related with CaM is the MLCK, a key regulatory enzyme in the process of smooth muscle relaxation–contraction events. The contractile activity in smooth muscle is initiated by a Ca^{2+}–CaM dependent self-phosphorylation of the MLCK (Webb, 2003). In the absence of Ca^{2+} and/or CaM, MLCK remains inactive because it binds to its own pseudosubstrate domain, which has sequence homology to the myosin light chain, its physiological substrate. However, upon CaM binding, this domain is removed from the active site, and the enzyme becomes active and self-phosphorylates (Filenko *et al*., 1997). As with the complex Ca^{2+}–CaM–PDE1, the Ca^{2+}–CaM–MLCK complex could be the target of novel drugs.

Considering that CaM and its protein–protein complexes represent the target of potential medication, usually known as CaM inhibitors. In this study, we analyzed both experimentally and theoretically the effect of the CaM inhibitor malbrancheamide (MBC) on three Ca^{2+}–CaM target protein or peptide complexes, namely, Ca^{2+}–CaM–PDE1A, Ca^{2+}–CaM–MLCK, and Ca^{2+}–CaM–peptide 1 derived from the human αII–spectrin (αII–spec). All these were carried out using the fluorescent biosensor *h*CaM M124C–*mBBr* (González-Andrade *et al*., 2009). In the first two cases, chlorpromazine (CPZ), a classical CaM inhibitor was also analyzed.

MATERIALS AND METHODS

Proteins and reagents

The fluorescent biosensor *h*CaM M124C–*mBBr* was purified and chemically modified with monobromobimane (*mBBr*) as previously described by González-Andrade *et al*., 2009. Purity was confirmed by SDS-PAGE, and the concentration was determined with the bicinchoninic acid method (Smith *et al*., 1985). The calcium/calmodulin-dependent 3′,5′-cyclic nucleotide phosphodiesterase 1A active human (PDE1A) and MLCK were obtained from Sigma-Aldrich (Sigma, St. Louis, MO, USA). Calmodulin binding peptide 1 with the sequence GVMPREETDSKTASPWKSARLMVHTVATFNSIKELNERWRSLQQLA (Cat. No. RP13247) derived of portion of the human αII–spectrin (αII–spec) from GenScript Corporation (GenScript, Piscataway, NJ, USA). CPZ was obtained from Sigma (Sigma, St. Louis, MO, USA), and the alkaloid MBC was extracted and isolated from a stock culture of the fungi *M. aurantiaca* as previously illustrated by Figueroa *et al*., 2011.

Steady-state fluorescence

All measurements were conducted with an ISS–PC1 spectrofluorometer (ISS, Champaign, IL) with sample stirring at 37 °C. The biosensor fluorescence *h*CaM M124C–*mBBr* (1 μM) was incubated in buffer (50 mM of sodium acetate [pH 5.1] and 10 μM of $CaCl_2$). Fluorescence emission spectra were acquired with excitation and emission slit widths of 4 and 8 nm, respectively. The excitation wavelength was 381 nm, and emission wavelengths of 415–550 nm were measured. The fractional saturation (y) of the *h*CaM M124C–*mBBr*–protein complex with peptide and/or compounds (CPZ or MBC) was calculated by changes in fluorescence upon ligands binding according to $y = (F - F_0)/(F_\infty - F_0)$, where F_∞ represents the fluorescence intensity at full saturation with the ligands, y is plotted as a function of the Ca^{2+}–CaM/inhibitor, Ca^{2+}–CaM–protein/inhibitor, and Ca^{2+}–CaM–peptide/inhibitor or Ca^{2+}–CaM–inhibitor/peptide relation (L); the apparent dissociation constant (K_d) and stoichiometry (S) were obtained by fitting to the equation:

$$y = \frac{(1 + K_d/S + L/S) - \sqrt{(1 + K_d/S + L/S)^2 - 4L/S}}{2}$$

where y represents the fractional degree of fluorescence intensity at 470 nm, K_d is the apparent dissociation constant for the ligands, L is the protein or protein complex/ligand relation, and S is the stoichiometric. Data were analyzed using the Origin version 8.0 program (OriginLab, Northampton, MA).

Modeling of PDE1A

The structural model of PDE1A isoform 1 from *Homo sapiens* was built up using comparative and *ab initio* modeling. The PDE1A1 (gi 21361262, ResSeq NP_005010.2) from *Homo sapiens* comprises 545 amino acid residues. The sequence was retrieved from the NCBI (Sayers *et al*., 2010). RefSeq database (http://www.ncbi.nlm.nih.gov/protein/NP_005010.2, accessed on March 9, 2011) and a suitable template were searched using the Blast service at NCBI (Sayers *et al*., 2010). The human PDE1B (PDB entry 1TAZ) has nearly 60% similarity, but covers only 70% of the full amino acid sequence of the target, and does not comprise the CaM binding domains. Therefore, three full models were accomplished using the Rosetta software (Kaufmann *et al*., 2010), the SAM-T08 server (available at http://compbio.soe.ucsc.edu/SAM_T08/T08-query.html) (Karplus *et al*., 2003), and Pro-Sp3-TASSER server (available at http://cssb.biology.gatech.edu/skolnick/webservice/pro-sp3-TASSER/index.html) (Zhou and Skolnick, 2009). The ROSETTA model was rebuilt in regions surrounding insertions and deletions in the sequence alignment. Missing loops were built using the fragment insertion or the randomization of the angles φ and ψ, followed by one of the loop closure algorithms in Rosetta, such as descent cyclic coordinate or kinematic closure. In the SAM-T08 and Pro-SP3-TASSER predictions, structural defects are frequent, such as atom clashes and/or long bonds. Therefore, these models were then minimized with Hyperchem™ 8.0 release 8.0.6 under AMBER force field, to correct structural defects, such as atom clashes and/or long bonds, which are frequent in the predictions from these servers. The minimized models were further refined using the protocol ROSETTA v3.2 fast-relax (Raman *et al*., 2009). The final geometries were verified from the analysis of per-residue energy reports in the AMBER and ROSETTA force field, and their structural consistency was examined with ProCheck (stereochemical quality analysis software; Laskowski *et al*., 1993), Verify-3D (structure evaluation software; Luthy *et al*., 1992), and Whatcheck (protein verification tools software; Hooft *et al*., 1996) computer programs. Then, all models were scored with the Rd.HMM protocol to recover the model with the highest appropriateness score, having an in-frame, gapless Rd.HMM alignment to the target amino acid sequence, and not producing a better alignment to other distantly related sequences, such as, for instance, the

amino acid sequences of the templates selected by SAM or their corresponding homologues (Martinez-Castilla and Rodriguez-Sotres, 2010). The model with the highest Rd.HMM score against the target sequence was the ROSETTA model, and this model was selected.

Protein–protein docking

To prepare the structures for docking, the unbound structures were placed in the zones close of interaction described in the literature for these proteins (Persechini and Kretsinger, 1988; Goraya and Cooper, 2005; Yosef *et al*., 2009), and the resulting structure was used as the starting structure for local docking. The structures for Ca^{2+}–CaM–PDE1A complex were the CaM structure refined at 1.7 Å resolution (PDB code 1CLL.pdb) (Chattopadhyaya *et al*., 1992) and the model obtained by molecular modeling of PDE1A; for Ca^{2+}–CaM–MLCK complex, structures were the same as in previous case for the CaM and chain A of the human MLCK Loc340156 (PDB code 2X4F.pdb) to MLCK. All structures were rebuilt and refined previously using the idealization application of Rosetta v3.2 software. The docking was carried out with the RosettaDock v3.2 employing two methods: a low-resolution rigid-body docking and thereafter followed by a high-resolution refinement stage for side chain conformational sampling and backbone relaxation to generate 1000 decoys (candidate structures) from each method. The rigid-backbone docking protocol employed was as identical as the traditional RosettaDock method, which involves 500 steps of low-resolution rigid-body Monte Carlo (MC) search, followed by 50 cycles of high-resolution Monte Carlo Minimization (MCM) refinement. The low-resolution rigid-body search consisted in the rotation and translation of one protein around the surface of the other with movements chosen from a Gaussian distribution centered at 5 and 0.7 Å. Each conformation is scored using the low-resolution energy function based on residue pair interaction statistics, residue environment statistics, and van der Waals attractive and repulsive terms. Each cycle, the high-resolution MCM refinement, consists of a 0.1 Å random rigid-body translation, Monte Carlo-based side chain roamers sampling (packing), and gradient-based rigid-body translation (Kaufmann *et al*., 2010; Chaudhury *et al*., 2011). All calculations were made using a parallel distributed memory supercomputer (KanBalam System, Dirección General de Cómputo y de Tecnologías de Información y Comunicación, UNAM), which contains 1368 processors AMD Opteron, around three terabyte of memory and 160 terabyte of disk storage (http://www.super.unam.mx/). The analysis of the docking was made with the program PyMOL 1.3 (DeLano, 2004) and LIGPLOT v.4.0 (Wallace *et al*., 1995).

Determination of accessible surface area

The accessible surface area (ASA) of the PDE1A, MLCK, Ca^{2+}–CaM, and of the Ca^{2+}CaM–PDE1A and Ca^{2+}CaM–MLCK complexes were calculated by the Lee–Richards algorithm implemented in NACCESS 2.1.1 software (Lee and Richards, 1971). ASA is calculated using the "rolling ball" algorithm, which uses a sphere (representing the solvent) of a particular radius to "probe" the surface of the molecule. A typical value of a "probe radius" is 1.4 Å, which approximates the radius of a water molecule. The residues at the interface of the complexes were defined as the residues that show a difference in the ASA upon complexation.

Protein–peptide:ligand and Protein–protein:ligand docking

Docking was carried out using the X-ray structure of Ca^{2+}–CaM and Ca^{2+}–CaM–αII–spec complex (1CLL.pdb and 2FOT.pdb) as well as the Ca^{2+}–CaM–PDE1A and Ca^{2+}–CaM–MLCK complex obtained from RosettaDock. The ligands (CPZ and MBC) were built using the program HyperChem™ 8.0 release 8.0.6. The protein complex and the ligand were further prepared using the utilities implemented by AutoDockTools 1.5.4, revision 30 (http://mgltools.scripps.edu/). The protein complex was prepared for AutoDock by addition of all hydrogen atoms, Kollman united-atom partial charges, and the ligands were prepared by computation of atom charges with the Gasteiger–Marsilli formalism and assignment of active torsion groups, which was carried out with AutoDockTools. Blind docking was carried out using AutoDock4 version 4.2 software (http://autodock.scripps.edu/) (Morris *et al*., 1998; Huey *et al*., 2007) using the default parameters: number of individuals in population (150), maximum number of energy evaluations (2.5 million), maximum number of generations (27 000), rate of gene mutation (0.02), rate of crossover (0.8), and 1000 runs for docking. Electrostatic grid maps were generated for each atom type in the ligands utilizing the auxiliary program AutoGrid4 part of the software AutoDock4. Calculations were made using the computing facilities described previously (KanBalam cluster). Each run required an average of 0.5 min. The analysis of the docking was accomplished with AutoDockTools using cluster analysis, LIGPLOT, and PyMOL software.

RESULTS AND DISCUSSION

Protein–protein interaction (Ca^{2+}–CaM–PDE1A and Ca^{2+}–CaM–MLCK)

Calmodulin is a regulatory protein involved in numerous cellular processes mediated by calcium. The concentration of Ca^{2+} varies in different cellular compartments and states producing different amounts of Ca^{2+}–CaM complex, which in turn modulates the dissimilar CaM target enzymes that will finally determine cellular responses. In general, the activation mechanism of CaM involves the exposure of hydrophobic patches when calcium ions bind followed by the recognition of these domains by the target proteins. Trifluoroperazine, CPZ, MBC, KAR-2, and other inhibitors bind directly to CaM, blocking its interaction with its target proteins (Brooks *et al*., 1985). However, the direct influence of different CaM inhibitors on the complexes Ca^{2+}–CaM target proteins has been assessed, although indirect effects have been evaluated throughout functional enzymatic assays (Sharma *et al*., 1997; Figueroa *et al*., 2011).

Determination of the binding affinity of MBC and CPZ with the complexes Ca^{2+}–CaM–PDE1A and Ca^{2+}–CaM–MLCK

The affinity of MBC and CPZ on Ca^{2+}–CaM, Ca^{2+}–CaM–PDE1A, and Ca^{2+}–CaM–MLCK complexes were determined using the fluorescent biosensor *h*CaM M124C–*mBBr*. Figure 1 shows the resulting CPZ and MBC titration curves, and the lines resulting from fitting the data to the binding model of Ca^{2+}–*h*CaM M124C–*mBBr*–PDE1A and Ca^{2+}–*h*CaM M124C–*mBBr*–MLCK (with 1:1 stoichiometry of protein:protein). The results indicate that both CPZ and MBC quenched the fluorescence of the complexes, providing direct evidence that CPZ and MBC perturb the Ca^{2+}–CaM–PDE1A and Ca^{2+}–CaM–MLCK complexes. Therefore, these compounds may be inhibiting CaM by directly binding to

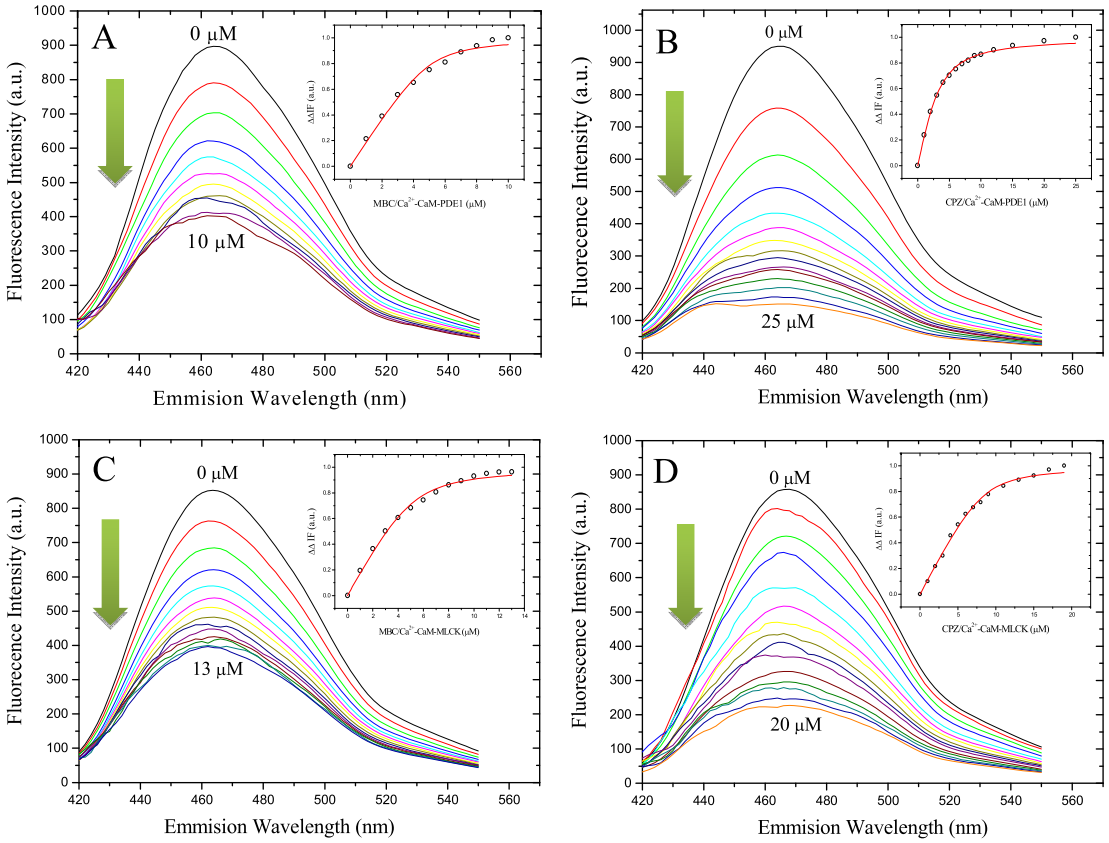

Figure 1. Fluorescence spectra and titration curves of the complex *h*CaM M124C–*mBBr* enzyme. (A) Ca^{2+}–*h*CaM–PDE1A–MBC, (B) Ca^{2+}–*h*CaM–PDE1A–CPZ, (C) Ca^{2+}–*h*CaM–MLCK–MBC, and (D) Ca^{2+}–*h*CaM–MLCK–CPZ. Green arrows indicate the quenching of fluorescence of the biosensor by adding the ligands. Protein concentration used was 1.0 μM, and the buffer was 50 mM of sodium acetate (pH 5.1) at 37 °C and 10 μM $CaCl_2$. Samples were excited at 381 nm, and emission spectra were recorded from 415 to 550 nm. The absolute changes of maximal fluorescence emission were corrected for light scattering effects and plotted relative changes in intensity (ΔΔIF) against the ligand to total protein–protein complex ratio (insets). The continuous line in the insets comes from the fitting of data to the binding model (equation in methods section) to obtain the K_d and the stoichiometry ratio. The resulting parameter estimates are given in Table 1.

their complexes with the target protein and inducing conformational changes leading to a non-functional complex or to Ca^{2+}–CaM target dissociation. These results are consistent with previous kinetic analysis that revealed that MBC was a competitive inhibitor of CaM (González-Andrade *et al*., 2009), but it may also help to explain how a ligand can destabilize protein–protein complexes and act effectively as a drug *in vivo*. Although the molecular target of the CaM inhibitors has been clearly established, the mechanistic details of their action will require further consideration. In addition, the outcomes indicated that the two ligands here tested interact differentially with the complexes CaM forms, depending on the partner protein. Thus, MBC exhibited higher affinity for the complex Ca^{2+}–CaM–PDE1A ($K_d = 0.28$) than for Ca^{2+}–CaM–MLCK ($K_d = 0.55$) or Ca^{2+}–CaM ($K_d = 1.11$) alone. On the other hand, as compared with MBC, CPZ showed slightly less affinity for all three complexes (Table 1).

Protein–peptide–ligand interaction

The affinity of Ca^{2+}–CaM for many peptides (taken from their targets) is higher than its affinity for smallest molecules acting as CaM inhibitors (Sharma, 2003). The possible structural grounds for this high affinity can be derived from the CaM–peptide complex structures, determined by X-ray or NMR analyses, and related to the extensive binding interface produced when the two globular domains of CaM embrace the target peptide (Shifman and Mayo, 2002) (Figure 2). The complexes show a substantial amount of hydrophobic surface area burial between Ca^{2+}–CaM and the target peptides, and it has been suggested that methionine side chains, abundant in the CaM–peptide interface, play an important role in Ca^{2+}–CaM target recognition mechanism and therefore mediate the high affinity. To understand the basis of this mechanism, we made experiments of competition between Ca^{2+}–CaM, MBC, and αII–spec peptide using the fluorescence biosensor of *h*CaM M124C–*mBBr* and docking studies with Ca^{2+}–CaM–αII–spec complex, CPZ, and MBC. The αII–spec peptide, a high affinity CaM target, contains cleavage sites for μ-calpain, caspases 2, 3, and 7 and the recently identified Pet toxin proteinases (Simonovic *et al*., 2006).

Determination of the binding affinity of MBC with the complex Ca^{2+}–CaM–αII–spec

The binding properties of MBC with the complex Ca^{2+}–CaM–αII–spec were also observed with the same *h*CaM–M124C–*mBBr* fluorescent-engineered biosensor. The fluorescence titration curves and binding parameters for Ca^{2+}–CaM–αII–spec, Ca^{2+}–CaM–αII–spec-MBC, and Ca^{2+}–CaM–MBC–αII–spec are shown in Figure 3 and Table 1. In the case of αII–spec, the peptide showed a higher affinity for Ca^{2+}–*h*CaM M124C–*mBBr* ($K_d = 2.55 \pm 1.75$ pM),

Table 1. Binding parameters (quenching fluorescence) and energy values (kcal mol^{-1}) of interactions (docking) of Ca^{2+}–CaM target protein complexes

	Fluorescence quenching			Docking	
Complexes	Ligand	K_d[a] (μM)	Stoichiometry	K_i[b] (μM)	EFEB[c] (kcal/mol)
Ca^{2+}–CaM	MBC	1.11 ± 0.08	2.0 ± 0.1	0.791	−8.32
Ca^{2+}–CaM	CPZ	1.43 ± 0.09	0.6 ± 0.08	4.54	−7.29
Ca^{2+}–CaM	αII–spec	2.55×10^{-6}	0.6 ± 0.02	–	–
Ca^{2+}–CaM–PDE1A	MBC	0.28 ± 0.08	5.0 ± 0.3	0.183	−9.19
Ca^{2+}–CaM–PDE1A	CPZ	1.10 ± 0.09	3.0 ± 0.3	1.86	−7.82
Ca^{2+}–CaM–MLCK	MBC	0.55 ± 0.08	5.1 ± 0.3	0.134	−9.37
Ca^{2+}–CaM–MLCK	CPZ	0.61 ± 0.11	8.3 ± 0.4	0.493	−8.60
Ca^{2+}–CaM–MBC	αII–spec	2.72×10^{-6}	0.5 ± 0.01	–	–
Ca^{2+}–CaM–αII–spec	MBC	–	–	2.96	−7.54
Ca^{2+}–CaM–αII–spec	CPZ	–	–	52.68	−5.84

[a]Apparent dissociation constants.
[b]Estimated inhibition constants.
[c]Binding Free Energy.

which is roughly about two orders of magnitude higher that the affinity of MBC for Ca^{2+}–*h*CaM M124C–*mBBr*, as judging from the quenching of extrinsic fluorescence (Figure 4A) and from the increase in intrinsic fluorescence (Figure 4B). The quenching is mainly attributed to the direct interaction between the TRP1192 of the peptide and the biosensor probe (Figure 2). This last argument is consistent with available crystallographic data, which revealed that the tryptophan side chain forms a hydrogen bond with the carbonyl oxygen of Met124 of CaM (Simonovic *et al.*, 2006). The increase in intrinsic fluorescence ($\lambda_{ex} = 295$ nm, $\lambda_{em} = 315$–350 nm) is also directly proportional to the amount of peptide added (Figure 4B), but the signal intensity is considerably weaker. We emphasize here the value of using a fluorescent engineered biosensor to measure the K_d for different ligands. The K_d of αII–spec peptide to Ca^{2+}–CaM is consistent with those values previously reported for other CaM–peptide complexes (Shifman and Mayo, 2002). In addition, competition experiments were made between Ca^{2+}–CaM, MBC, and αII–spec peptide. Figure 4A revealed that titration of Ca^{2+}–*h*CaM M124C–*mBBr* with αII–spec (0–293 nM) quenched the extrinsic fluorescence; when MBC (up to 16 μM) was added, the fluorescent signal showed no further changes. However, when the experiment was carried out titrating Ca^{2+}–*h*CaM M124C–*mBBr*–MBC complex with αII–spec, the fluorescent signal was quenched, indicating that the αII–spec peptide appears to be capable of displacing MBC, keeping practically the same affinity for Ca^{2+}–CaM (K_d 2.72 ± 1.6 pM; Figure 3B and Table 1). Thus, the ligand with lower affinity (MBC) was unable to displace the peptide of the Ca^{2+}–CaM–αII–spec complex, as expected for a competitive binding mechanism. Consequently, these results demonstrate that the molecular recognition and binding of ligands is a very dynamic process.

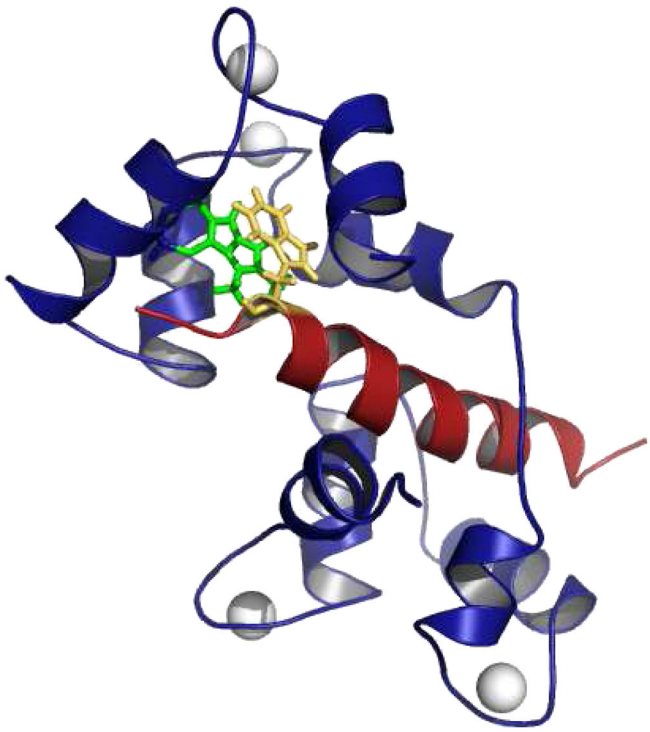

Figure 2. Structural model of *h*CaM M124C–*mBBr* in presence of the αII–spec peptide. This model was developed from X-ray structure 2FOT. pdb. A mutation *in silico* was made (M124C), and subsequently, *mBBr* was covalently attached to the cysteine thiol group. A geometric optimization using Hyperchem™ Professional version 8.0 software was made only at the mutated residue and the bimane moiety. The blue density cartoon represents CaM, the red firebrick cartoon depicts the αII–spec peptide, the green sticks represent *mBBr*, the yellow-orange sticks represent TRP1192, and the white balls indicate the Ca^{2+}. The structures were drawn using PyMOL (DeLano, 2004).

Structural modeling of PDE1A

The crystal structure of PDE1A is not available; molecular modeling tools were used to build the structural model of PDE1A, which in turn was used for predicting Ca^{2+}–CaM–PDE1A interaction by throughout docking analysis (see Methods section). The protein was modeled in four steps: (i) identification of a suitable structural template; in this case, the calcium/calmodulin-dependent 3′,5′-cyclic nucleotide phosphodiesterase 1B (NCBI gi 4505677; PDB 1TAZ); (ii) alignment of target sequence and template structure; (iii) model building; and finally, (iv) model quality evaluation. Three models were obtained for PDE1A (NCBI gi

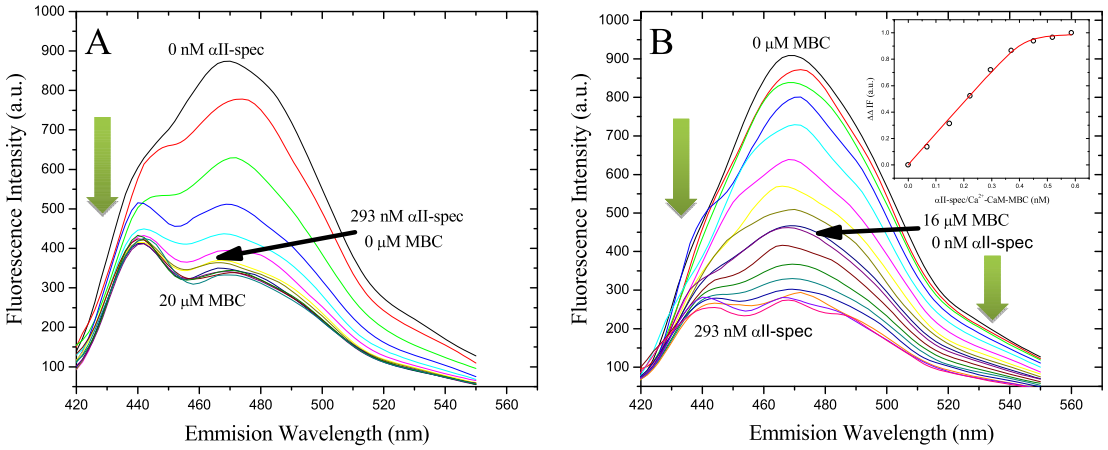

Figure 3. Fluorescence spectra of Ca^{2+}–*h*CaM M124C–*mBBr* adding αII–spec peptide and MBC and inversely. (A) Ca^{2+}–*h*CaM M124C–*mBBr* fluorescence, upon the addition of αII–spec peptide to 259 nM, followed by addition of MBC to 20 μM. (B) Biosensor *h*CaM fluorescence upon addition of MBC at saturation (0–16 μM), with the subsequent addition of αII–spec peptide to 293 nM. Green arrows indicate the quenching of fluorescence of the biosensor by adding the ligands, and black arrows indicate the change of ligand added. Experiment conditions were as indicated in Figure 1.

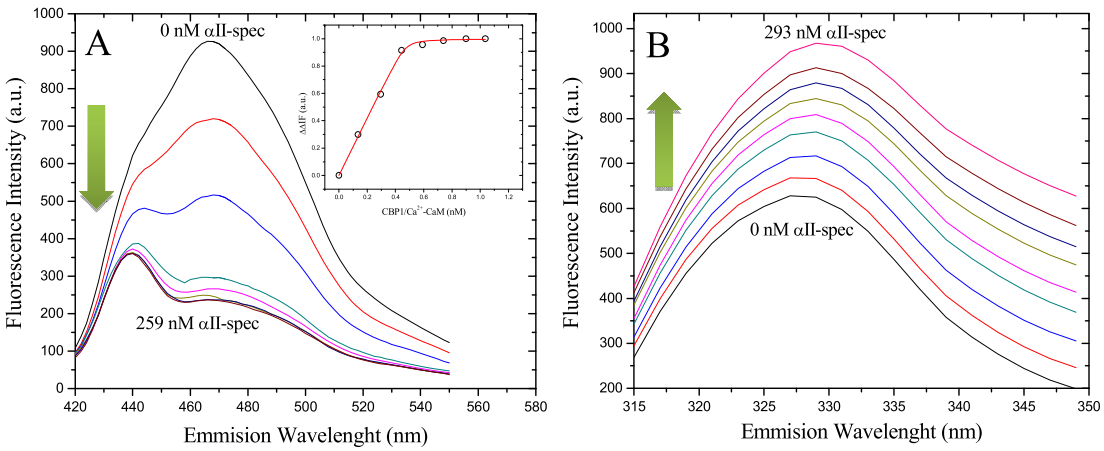

Figure 4. Fluorescence spectra and titration curves of Ca^{2+}–*h*CaM M124C–*mBBr* with the αII–spec peptide. (A) Sample was excited at 381 nm, and emission spectra were recorded from 415 to 550 nm. The absolute changes of maximal fluorescence emission were plotted against the ration αII–spec/protein total and fitted to the binding equation model to obtain the K_d. (B) Fluorescence spectra of the titration of αII–spec peptide (0–259 nM), $\lambda_{ex} = 295$ nm and $\lambda_{em} = 315$–350 nm. Protein concentration used was 250 nM, and the buffer was 50 mM of sodium acetate (pH 5.1) at 37 °C and 10 μM $CaCl_2$.

21361262) using a combination of *ab initio* and comparative modeling with the Rosetta software (Kaufmann *et al.*, 2010), or through the SAM-T08 and Pro-Sp3-TASSER servers. Rosetta is considered a fusion between comparative modeling and *ab initio* because it uses available templates and assembles the remaining segments forms a large set of fragments. In addition, the models from SAM-T08 will use distant sequence homology supported by hidden Markov models, to obtain possible matches for the unknown regions. All three models were refined using molecular mechanics and their structural consistency was analyzed as described in methods section. After this structural refinement and quality evaluation, their biological appropriateness was tested using the Rd.HMM protocol (Martinez-Castilla and Rodriguez-Sotres, 2010). The best model recovered the target sequence from the NCBI-nr (gi|21361262|ref|NP_005010.2|; calcium/calmodulin-dependent 3′,5′-cyclic nucleotide phosphodiesterase 1A isoform 1 [*Homo sapiens*]) with a score of 365 (67.0% of sequence length), and *E*-value of 1.5×10^{-103} at the top of the list. The insole sequence was not on the list as its score was negative. In any case, the Rd. HMM appropriateness score gives the final model good confidence because we have not found yet any false positive with this protocol. Occasionally, the Rd.HMM protocol may give false negatives, that is, acceptable models rendering low scores, but clearly not the case here, because the final three-dimensional coordinates from the best structural model (generated by Rosetta *ab initio*) produced a good score for the target sequence (gi|21361262|ref|NP_005010.2), as shown in Table S1 (Supporting Information) where all first 20 best scores were homologues of PDE1 isoforms from higher vertebrates (only 1–5, 10, and 20 are shown). Figure S1 shows the final Rd.HMM alignment, with three notable features: (i) The HMMer model consensus and the target sequence match position by position to each other, with no gaps in the middle. (ii) There are conserved (+ and lowercase letters) and highly conserved (uppercase letters) positions along the whole sequence length, including the N and C-terminal regions, with a distribution marks similar to that in the core part (where the starting template was similar). (iii) The top hit was the target sequence, and the sequence from the template was found nearly at the bottom of

the list, with negative score and no statistical significance. The alignment of the target sequence to the structural Rd.HMM was free of gaps (misalignments and/or frame shifts), and its Rd.HMM score was well above the minimum score for an acceptable model (30% of sequence length, or 163.5). These data indicated that the atomic backbone coordinates of the model built were a better host for the PDE1A1's amino acid sequence than for the amino acid sequence of the closest known structure (negative Rd.HMM score), thus representing a biologically appropriate approximation to the three-dimensional structure, with high structural quality. Figure S2 shows the superposition of the model obtained for PDE1A with the X-ray structure of catalytic domain of human phosphodiesterase 1B and the corresponding sequence alignment.

Protein–protein dockings and determination of interfaces in the complexes

With the aim of generating structural models of the interactions of Ca^{2+}–CaM–PDE1A and Ca^{2+}–CaM–MLCK complexes, protein–protein docking studies using the RosettaDock protocol were accomplished (Chaudhury *et al*., 2011). This tool is part of the Rosetta 3.2 software package (http://www.rosettacommons.org). One thousand structures of each complex were performed and analyzed on the basis of their interface energy (Score) and root mean squared deviation (RMSD) of the Cα atomic coordinates from the initial model; the best docked complex was subsequently refined having another 1000 new structures and analyzed as before (interface energy and RMSD). Figure 5 shows the results of the low-resolution rigid-body docking as a scatterplot and Figure S3 of the high-resolution refinement; therefore, we elected the best model based on the scores. The average computation time required for each run was 1.12 and 1.68 min for Ca^{2+}–CaM–MLCK and Ca^{2+}–CaM–PDE1A, respectively (about 30 h for complex). To find the interfaces determinant to the protein–protein interaction per residue, the ASA by complex was calculated for each case using NACCESS 2.1.1 software. The interface between proteins was defined from Van der Waals contacts (atom distances below the sum of their Van der Waals 1.125 Å), polar interactions (polar atoms at distances below 4.7 Å), and hydrophobic interaction (hydrophobic amino acid residues with side chains closer than 4.7 Å) (Mihel *et al*., 2008). ASA changes per residue upon protein complex formation were used as a measure of interaction strength. Table S2 shows the interface residues involved in each complex formation, where most of the residues are hydrophobic character. In the case of CaM, this is not new because the X-ray structure of Ca^{2+}–CaM bound to different targets has revealed CaM hydrophobic patches (Yang *et al*., 2004; Menyhard *et al*., 2009).

Docking studies protein–peptide:ligand and protein–protein:ligand.

To generate a binding model to locate the most likely and estimate a theoretical inhibition constant (K_i) for CPZ and MBC with Ca^{2+}–CaM, Ca^{2+}–CaM–αII–spec, Ca^{2+}–CaM–MLCK, and Ca^{2+}–CaM–PDE1A, a molecular docking study was carried out using the program AutoDock4, made 1000 runs for each complex ligand. Each run required an average of 0.5 min. These program calculates a K_i from docking energy using the following equation: $K_i = \exp(\Delta G * 1000)/RT)$, where ΔG = docking energy; $R = 1.98719\ \text{cal K}^{-1}\ \text{mol}^{-1}$, $T = 298.15$ K, and K_i = estimated inhibition constant, predicting the possible site of interaction of the ligands at the complexes. An analysis of the intermolecular interactions of all the complexes including hydrophobic and hydrogen-bonding contacts were made using LIGPLOT to select the lowest energy states. The results are shown in Table 1 and Figures 6, 7, and S4–S9. The K_i estimate to the ligands (MBC and CPZ) had good correlation with experimental data, for example, for MBC with the Ca^{2+}–CaM and Ca^{2+}–CaM–PDE1A complexes, the K_d and K_i were 1.11 and 0.79, and 0.28 and 0.18 μM, respectively, and for the CPZ with the Ca^{2+}–CaM–PDE1A and Ca^{2+}–CaM–MLCK complexes, K_d and K_i were 1.10 and 1.86, and 0.61 and 0.49 μM, respectively. Figure S10 shows an example of clustering histogram (CaM–MLCK–MBC complex), where one can notice that the best energetically clusters are not always the most abundant. This may be related to the search area in the target and its size as well as the existing energy barrier along the molecular mesh. MBC and CPZ showed more conformational clusters when docked to Ca^{2+}–CaM–protein complex than when docked to Ca^{2+}–CaM alone. This makes sense by giving a larger surface area available for contact. The results of docking to Ca^{2+}–CaM indicate that the protein has two preferential interaction regions for binding these ligands, both rich in hydrophobic amino acids and located at each lobe of Ca^{2+}–CaM (Figure S5). For the Ca^{2+}–CaM–αII–spec complex, the same sites of interaction are observed. However, a larger number of both, hydrophobic interactions as hydrogen bonds, were observed (Figure S6 and S7). In the Ca^{2+}–CaM–MLCK and Ca^{2+}–CaM–PDE1A

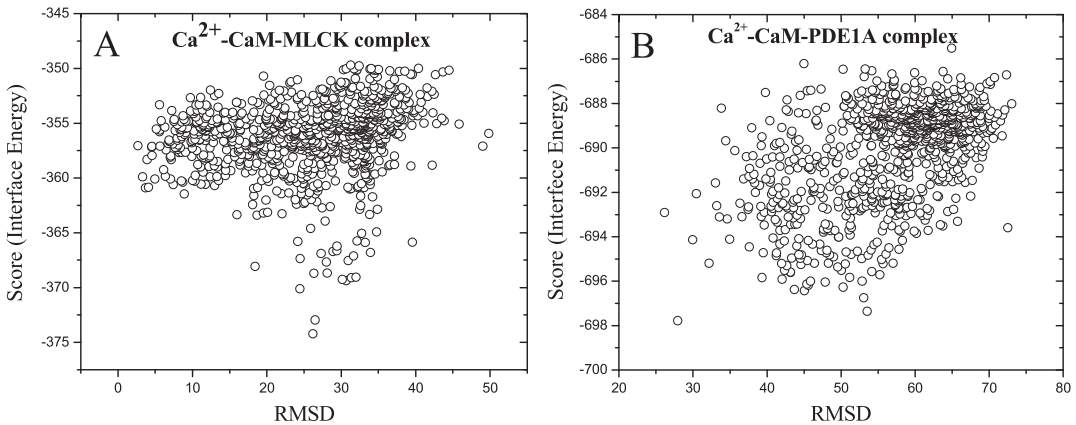

Figure 5. Result of the low-resolution docking. Score (interface energy) and root mean squared deviation (RMSD) of the Cα atomic coordinate scatter plots for representative (A) Ca^{2+}–CaM–PDE1A complex and (B) Ca^{2+}–CaM–MLCK complex. In this case, the less scores represent the best results of the docking.

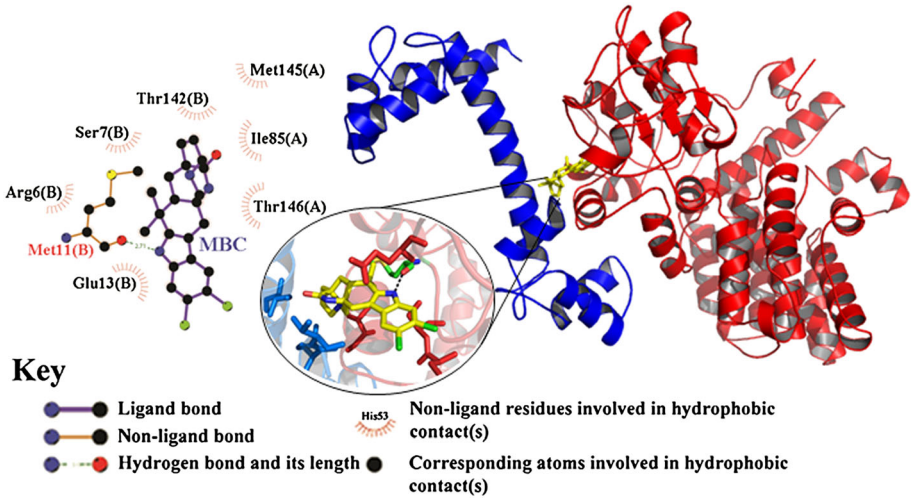

Figure 6. Structural models of CaM–PDE1A–MBC complex. Shown on the right is the complex in blue cartoon, red cartoon, and yellow stick, the CaM, PDE1A, and MBC, respectively. The pocket of binding is shown in the center. Shown on the left is the two-dimensional representation of CaM–PDE1A–MBC interactions resulting from the docking, with residues indicated for CaM(A) and PDE1A(B). The images were made with PyMOL and LIGPLOT.

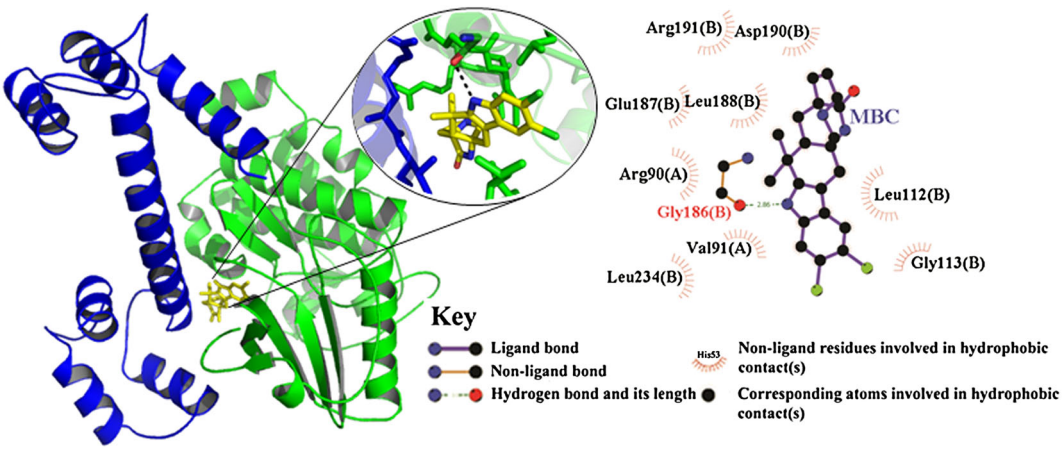

Figure 7. Structural models of CaM–MLCK–MBC complex. Shown on the left is the complex in blue cartoon, green cartoon, and yellow stick, the CaM, PDE1A, and MBC, respectively. Shown in the center is the pocket of binding in a zoom. Shown on the right is the two-dimensional representation of CaM–MLCK–MBC interactions from the docking, with residues indicated for CaM(A) and MLCK(B).

complexes, predicted binding sites are located at the interface of the protein–protein complexes (Figure 6, 7, S8, and S9). Figure 6 shows the docking of Ca^{2+}–CaM–MLCK–MBC complex where the best interaction site is located at the interface between the two proteins. Such contact may lead to a structural change in both proteins and perturb its interaction. Considering that the interfaces in protein–protein complexes play a key role in their stabilization, the observed ligand's binding may explain its ability to produce a therapeutic effect *in vivo*, because a pure competitive displacement of the MLCK from its complex with CaM by CPZ is unlikely to take place, given its much lower affinity constant.

CONCLUSION

In summary, we have studied the affinity of two anti-CaM compounds on Ca^{2+}–CaM target protein complexes and have observed that the affinity of these compounds varies depending on the complex so that a CaM inhibitor could have a differential effect on the many Ca^{2+}–CaM target protein complexes. These differences in affinity could be useful to the development of drugs with specificity for particular Ca^{2+}–CaM target complexes, which may then be useful for the treatment of pathological processes where CaM and that particular target protein are involved. In addition, competition experiments with MBC and αII–spec on Ca^{2+}–CaM revealed a competitive antagonism between both ligands showing for the latter a higher affinity. Therefore, small molecules (inhibitors) can act on protein complexes with unsimilar affinity. With the inhibitors and complexes tested here, the relative affinity for the complexes and for the free protein differed, but this might be applicable to other CaM inhibitors and other Ca^{2+}–CaM target complexes, with important implications for the search of new drugs. Docking studies indicated that the interface plays a key role and affect the conformational equilibrium of protein complexes associated with CaM. Therefore, this type of phenomenon can be related directly with the both physiological and pathological effects where CaM participates, through conformational equilibriums between proteins and ligands that interact with CaM.

Acknowledgements

This work was supported by grants from DGAPA-UNAM (IN218110) and Instituto Nacional de Medicina Genómica (project #108). We thank Araceli Pérez for her valuable technical assistance. The authors are very grateful to Dr. A. Olson and his colleagues at the Scripps Research Institute for providing AutoDock, Dr. D. Baker for supplying Rosetta software and Dr S. Schooling Director PS&E, UCL Business PLC for providing LigPlot software. We are indebted to Dirección General de Cómputo y de Tecnologías de Información y Comunicación, UNAM, for providing the resources to carry out computational calculations through KanBalam System.

REFERENCES

Aramburu J, Rao A, Klee CB. 2000. Calcineurin: from structure to function. *Curr. Top. Cell. Regul.* **36**: 237–295.

Beavo JA. 1995. Cyclic nucleotide phosphodiesterases: functional implications of multiple isoforms. *Physiol. Rev.* **75**: 725–748.

Bjork J, Lundberg S, Backman L. 1995. Characterization of the binding of calmodulin to non-erythroid spectrin. *Eur. J. Cell Biol.* **66**: 200–204.

Bouche N, Yellin A, Snedden WA, Fromm H. 2005. Plant-specific calmodulin-binding proteins. *Annu. Rev. Plant Biol.* **56**: 435–466.

Brooks RL, Hunt JL, Macdonald JR, Poll JD, Waddington JC. 1985 Interference effects in the charge-induced spectrum of H-2 at 4.2 K. *Can. J. Phys.*. **63**: 937–940.

Buchwald P, Margolles-Clark E, Kenyon NS, Ricordi C. 2010. Organic dyes as small molecule protein–protein interaction inhibitors for the CD40–CD154 costimulatory interaction. *J. Mol. Recognit.* **23**: 65–73.

Chattopadhyaya R, Meador WE, Means AR, Quiocho FA. 1992 Calmodulin structure refined at 1.7 A resolution. *J. Mol. Biol.*. **228**: 1177–1192.

Chaudhury S, Berrondo M, Weitzner BD, Muthu P, Bergman H, Gray JJ. 2011. Benchmarking and analysis of protein docking performance in Rosetta v3.2. *PLoS One* **6**: e22477.

Chin D, Means AR. 2000. Calmodulin: a prototypical calcium sensor. *Trends Cell Biol.* **10**: 322–328.

Cho HJ, Xie QW, Calaycay J, Mumford RA, Swiderek KM, Lee TD, Nathan C. 1992 Calmodulin is a subunit of nitric oxide synthase from macrophages. *J. Exp. Med.* **176**: 599–604.

DeLano WL. 2004 Use of PYMOL as a communications tool for molecular science. *Abstr. Paper Am. Chem. S.* **228**: U313-U314.

Du J, Szabo ST, Gray NA, Manji HK. 2004 Focus on CaMKII: a molecular switch in the pathophysiology and treatment of mood and anxiety disorders. *Int. J. Neuropsychopharmacol.* **7**: 243–248.

Evans TI, Shea MA. 2009. Energetics of calmodulin domain interactions with the calmodulin binding domain of CaMKII. *Proteins* **76**: 47–61.

Figueroa M, González-Andrade M, Sosa-Peinado A, Madariaga-Mazon A, Del R-PF, Gonzalez MDC, Mata R. 2011. Fluorescence, circular dichroism, NMR, and docking studies of the interaction of the alkaloid malbrancheamide with calmodulin. *J. Enzyme Inhib. Med. Chem.* **26**: 378–385.

Filenko AM, Danilova VM, Sobieszek A. 1997. Smooth muscle myosin light chain kinase, supramolecular organization, modulation of activity, and related conformational changes. *Biophys. J.* **73**: 1593–1606.

González-Andrade M, Figueroa M, Rodriguez-Sotres R, Mata R, Sosa-Peinado A. 2009. An alternative assay to discover potential calmodulin inhibitors using a human fluorophore-labeled CaM protein. *Anal. Biochem.* **387**: 64–70.

Goraya TA, Cooper DM. 2005. Ca2+—calmodulin-dependent phosphodiesterase (PDE1): current perspectives. *Cell. Signal.* **17**: 789–797.

Hait WN, Lazo JS. 1986. Calmodulin: a potential target for cancer chemotherapeutic agents. *J. Clin. Oncol.* **4**: 994–1012.

Hooft RW, Vriend G, Sander C, Abola EE. 1996. Errors in protein structures. *Nature* **381**: 272.

Huber PA, El-Mezgueldi M, Grabarek Z, Slatter DA, Levine BA, Marston SB. 1996 Multiple-sited interaction of caldesmon with Ca(2+)-calmodulin. *Biochem. J.* **316**(Pt 2): 413–420.

Huey R, Morris GM, Olson AJ, Goodsell DS. 2007. A semiempirical free energy force field with charge-based desolvation. *J. Comput. Chem.* **28**: 1145–1152.

Junker JP, Rief M. 2009. Single-molecule force spectroscopy distinguishes target binding modes of calmodulin. *Proc. Natl. Acad. Sci. U.S.A.* **106**: 14361–14366.

Karplus K, Karchin R, Draper J, Casper J, Mandel-Gutfreund Y, Diekhans M, Hughey R. 2003. Combining local-structure, fold-recognition, and new fold methods for protein structure prediction. *Proteins* **53**: 491–496.

Kaufmann KW, Lemmon GH, Deluca SL, Sheehan JH, Meiler J. 2010. Practically useful: what the Rosetta protein modeling suite can do for you. *Biochemistry* **49**: 2987–2998.

Laskowski RA, MacArthur MW, Moss DS, Thornton JM. 1993. PROCHECK – a program to check the stereochemical quality of protein structures. *J. App. Cryst.* **26**: 283–291

Lee B, Richards FM. 1971. The interpretation of protein structures: estimation of static accessibility. *J. Mol. Biol.* **55**: 379–400.

Luthy R, Bowie JU, Eisenberg D. 1992. Assessment of protein models with three-dimensional profiles. *Nature* **356**: 83–85.

Martinez-Castilla LP, Rodriguez-Sotres R. 2010. A score of the ability of a three-dimensional protein model to retrieve its own sequence as a quantitative measure of its quality and appropriateness. *PLoS One* **5**: e12483.

Masciarelli S, Horner K, Liu C, Park SH, Hinckley M, Hockman S, Nedachi T, Jin C, Conti M, Manganiello V. 2004. Cyclic nucleotide phosphodiesterase 3A-deficient mice as a model of female infertility. *J. Clin. Invest.* **114**: 196–205.

Menyhard DK, Keseru GM, Naray-Szabo G. 2009 Calmodulin in complex with proteins and small molecule ligands: operating with the element of surprise; implications for structure-based drug design. *Curr. Comput. Aided Drug* **5**: 264–279.

Mihel J, Sikic M, Tomic S, Jeren B, Vlahovicek K. 2008. PSAIA – protein structure and interaction analyzer. *BMC Struct. Biol.* **8**: 21.

Morris GM, Goodsell DS, Halliday RS, Huey R, Hart WE, Belew RK, Olson AJ. 1998. Automated docking using a Lamarckian genetic algorithm and an empirical binding free energy function. *J. Comput. Chem.* **19**: 1639–1662.

Nairn AC, Picciotto MR. 1994. Calcium/calmodulin-dependent protein kinases. *Semin. Cancer Biol.* **5**: 295–303.

Oboyle KM, Waddington JL. 1985. Structural determinants of selective affinity for brain D-1 dopamine-receptors within a series of 1-phenyl-1h-3-benzazepine analogs of Sk-and-F-38393 and Sch-23390. *Eur. J. Pharmacol.* **115**: 291–295.

Persechini A, Kretsinger RH. 1988. Toward a model of the calmodulin-myosin light-chain kinase complex: implications for calmodulin function. *J. Cardiovasc. Pharm.* **12**(Suppl 5):S1-12.

Raman S, Vernon R, Thompson J, Tyka M, Sadreyev R, Pei J, Kim D, Kellogg E, DiMaio F, Lange O, Kinch L, Sheffler W, Kim BH, Das R, Grishin NV, Baker D. 2009. Structure prediction for CASP8 with all-atom refinement using Rosetta. *Proteins* **77**(Suppl 9): 89–99.

Rimmele S, Gierschik P, Joos TO, Schneiderhan-Marra N. 2010. Bead-based protein-protein interaction assays for the analysis of Rho GTPase signaling. *J. Mol. Recognit.* **23**: 543–550.

Sayers EW, Barrett T, Benson DA, Bolton E, Bryant SH, Canese K, Chetvernin V, Church DM, Dicuccio M, Federhen S, Feolo M, Geer LY, Helmberg W, Kapustin Y, Landsman D, Lipman DJ, Lu Z, Madden TL, Madej T, Maglott DR, Marchler-Bauer A, Miller V, Mizrachi I, Ostell J, Panchenko A, Pruitt KD, Schuler GD, Sequeira E, Sherry ST, Shumway M, Sirotkin K, Slotta D, Souvorov A, Starchenko G, Tatusova TA, Wagner L, Wang Y, John Wilbur W, Yaschenko E, Ye J. 2010. Database resources of the National Center for Biotechnology Information. *Nucleic Acids Res.* **38**: D5–16.

Seales EC, Micoli KJ, McDonald JM. 2006 Calmodulin is a critical regulator of osteoclastic differentiation, function, and survival. *J. Cell. Biochem.* **97**: 45–55.

Sharma RK. 2003 Diversity of calcium action in regulation of mammalian calmodulin-dependent cyclic nucleotide phosphodiesterase. *Indian J. Biochem. Bio.* **40**: 77–91.

Sharma RK, Wang JH, Wu Z. 1997. Mechanisms of inhibition of calmodulin-stimulated cyclic nucleotide phosphodiesterase by dihydropyridine calcium antagonists. *J. Neurochem.* **69**: 845–850.

Shifman JM, Mayo SL. 2002. Modulating calmodulin binding specificity through computational protein design. *J. Mol. Biol.* **323**: 417–423.

Simonovic M, Zhang Z, Cianci CD, Steitz TA, Morrow JS. 2006. Structure of the calmodulin alphall-spectrin complex provides insight into the regulation of cell plasticity. *J. Biol. Chem.* **281**: 34333–34340.

Smith PK, Krohn RI, Hermanson GT, Mallia AK, Gartner FH, Provenzano MD, Fujimoto EK, Goeke NM, Olson BJ, Klenk DC. 1985. Measurement of protein using bicinchoninic acid. *Anal. Biochem.* **150**: 76–85.
Sorensen BR, Shea MA. 1998. Interactions between domains of apo calmodulin alter calcium binding and stability. *Biochemistry* **37**: 4244–4253.
Wallace AC, Laskowski RA, Thornton JM. 1995 LIGPLOT: a program to generate schematic diagrams of protein-ligand interactions. *Protein Eng.* **8**: 127–134.
Wang H, Storm DR. 2003. Calmodulin-regulated adenylyl cyclases: cross-talk and plasticity in the central nervous system. *Mol. Pharmacol.* **63**: 463–468.
Webb RC. 2003. Smooth muscle contraction and relaxation. *Adv. Physiol. Educ.* **27**: 201–206.
Xia Z, Storm DR. 2005. The role of calmodulin as a signal integrator for synaptic plasticity. *Nat. Rev. Neurosci.* **6**: 267–276.
Yang C, Jas GS, Kuczera K. 2004 Structure, dynamics and interaction with kinase targets: computer simulations of calmodulin. *Biochim. Biophys. Acta* **1697**: 289–300.
Yosef E, Politi R, Choi MH, Shifman JM. 2009. Computational design of calmodulin mutants with up to 900-fold increase in binding specificity. *J. Mol. Biol.* **385**: 1470–1480.
Zhou H, Skolnick J. 2009. Protein structure prediction by pro-Sp3-TASSER. *Biophys. J.* **96**: 2119–2127.